Emergence of the Epidemic Methicillin-Resistant *Staphylococcus aureus* Strain USA300 Coincides with Horizontal Transfer of the Arginine Catabolic Mobile Element and *speG*-mediated Adaptations for Survival on Skin

Paul J. Planet,[a,b] Samuel J. LaRussa,[a] Ali Dana,[c] Hannah Smith,[a] Amy Xu,[a] Chanelle Ryan,[a] Anne-Catrin Uhlemann,[d] Sam Boundy,[e] Julia Goldberg,[a] Apurva Narechania,[b] Ritwij Kulkarni,[a] Adam J. Ratner,[a] Joan A. Geoghegan,[f] Sergios-Orestis Kolokotronis,[b,g] Alice Prince[a]

Division of Pediatric Infectious Diseases, Department of Pediatrics, Columbia University, College of Physicians and Surgeons, New York, New York, USA[a]; Sackler Institute for Comparative Genomics, American Museum of Natural History, New York, New York, USA[b]; Department of Dermatology, James J. Peters Veterans Affairs Medical Center, Bronx, New York, USA[c]; Department of Internal Medicine, Division of Infectious Diseases, Columbia University, College of Physicians and Surgeons, New York, New York, USA[d]; Department of Internal Medicine, Division of Infectious Diseases, Virginia Commonwealth University School of Medicine, Richmond, Virginia, USA[e]; Department of Microbiology, Moyne Institute of Preventive Medicine, Trinity College, Dublin, Ireland[f]; Department of Biological Sciences, Fordham University, Bronx, New York, USA[g]

ABSTRACT **The arginine catabolic mobile element (ACME) is the largest genomic region distinguishing epidemic USA300 strains of methicillin-resistant *Staphylococcus aureus* (MRSA) from other *S. aureus* strains. However, the functional relevance of ACME to infection and disease has remained unclear. Using phylogenetic analysis, we have shown that the modular segments of ACME were assembled into a single genetic locus in *Staphylococcus epidermidis* and then horizontally transferred to the common ancestor of USA300 strains in an extremely recent event. Acquisition of one ACME gene, *speG*, allowed USA300 strains to withstand levels of polyamines (e.g., spermidine) produced in skin that are toxic to other closely related *S. aureus* strains. *speG*-mediated polyamine tolerance also enhanced biofilm formation, adherence to fibrinogen/fibronectin, and resistance to antibiotic and keratinocyte-mediated killing. We suggest that these properties gave USA300 a major selective advantage during skin infection and colonization, contributing to the extraordinary evolutionary success of this clone.**

IMPORTANCE **Over the past 15 years, methicillin-resistant *Staphylococcus aureus* (MRSA) has become a major public health problem. It is likely that adaptations in specific MRSA lineages (e.g., USA300) drove the spread of MRSA across the United States and allowed it to replace other, less-virulent *S. aureus* strains. We suggest that one major factor in the evolutionary success of MRSA may have been the acquisition of a gene (*speG*) that allows *S. aureus* to evade the toxicity of polyamines (e.g., spermidine and spermine) that are produced in human skin. Polyamine tolerance likely gave MRSA multiple fitness advantages, including the formation of more-robust biofilms, increased adherence to host tissues, and resistance to antibiotics and killing by human skin cells.**

Received 17 October 2013 **Accepted** 20 November 2013 **Published** 17 December 2013

Citation Planet PJ, LaRussa SJ, Dana A, Smith H, Xu A, Ryan C, Uhlemann A-C, Boundy S, Goldberg J, Narechania A, Kulkarni R, Ratner AJ, Geoghegan JA, Kolokotronis S-O, Prince A. 2013. Emergence of the epidemic methicillin-resistant *Staphylococcus aureus* strain USA300 coincides with horizontal transfer of the arginine catabolic mobile element and *speG*-mediated adaptations for survival on skin. mBio 4(6):e00889-13. doi:10.1128/mBio.00889-13.

Editor Howard Shuman, University of Chicago

Copyright © 2013 Planet et al. This is an open-access article distributed under the terms of the Creative Commons Attribution-Noncommercial-ShareAlike 3.0 Unported license, which permits unrestricted noncommercial use, distribution, and reproduction in any medium, provided the original author and source are credited.

Address correspondence to Paul J. Planet, pjp23@columbia.edu.

Starting in the late 1990s, the USA300 lineage of methicillin-resistant *Staphylococcus aureus* (MRSA) underwent an extremely rapid expansion across the United States, replacing many other *S. aureus* strains (1). Since that time, it has become a major cause of skin and soft-tissue infections (2), community-acquired pneumonia, catheter-related bloodstream infections (3), and other systemic infections (4). The reason for the overwhelming success of the USA300 clone is not known, and there is a lively debate about the role that specific genetic factors play in the success and virulence of this lineage (5).

The 31-kb genomic island referred to as the arginine catabolic mobile element (ACME) may be particularly important for the fitness of USA300 strains (6). The ACME locus of USA300 is striking because it is virtually identical to highly prevalent genomic regions in *Staphylococcus epidermidis*, a colonizer of human skin (7–10), and ACME-like regions, most with markedly distinct gene contents and arrangements, are only occasionally found in non-USA300 *S. aureus* strains (11–14). These observations led to the assumption that the region was acquired from *S. epidermidis*, but the evolutionary direction, timing, and selective benefits of this horizontal event have not been investigated.

The ACME locus from USA300 strains is composed of at least 33 putative genes and two operons, referred to as *arc* and *opp* (Fig. 1A). The *arc* operon encodes genes that are thought to be involved

Downloaded from https://journals.asm.org/journal/mbio on 25 August 2022 by 138.5.97.228.

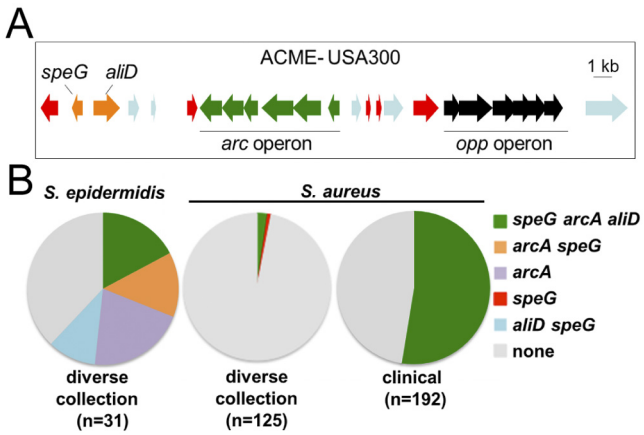

FIG 1 Prevalence of ACME genes in *S. aureus* and *S. epidermidis*. (A) Open reading frames (ORFs) of the 31-kb ACME. Integrase genes are red, *speG* locus genes are orange, *arc* genes are green, and *opp* genes are black. (B) Proportions of strains positive for ACME genes by either PCR or BLAST-based screening (see Materials and Methods). The first two pie charts represent a broad survey of geographically and genotypically diverse genomes (see the supplemental material). Note that in *S. epidermidis* the genes are found in different combinations, whereas in *S. aureus* the genes are only found together. The third pie chart shows presence of ACME genes in 192 environmental and clinical isolates (53), 137 of which were identified as belonging to the clonal complex of USA300 (ST8) by spa typing.

in arginine catabolism and has recently been shown to be important for survival of USA300 in acidic environments (6). The *opp* operon may encode an oligopeptide or metal transporter, and homologous genes have been implicated in virulence in *Streptococcus pyogenes* (15). Diep et al. (16) showed that deletion of ACME reduced the competitive fitness of USA300 in a rabbit bacteremia model, but others showed no virulence defect in rodent models of pneumonia or skin abscess (17).

Joshi et al. (18) showed that the ACME *speG* gene, which encodes a spermidine acetyltransferase (SpeG), confers the ability to survive levels of the polyamines spermidine and spermine that are lethal for other strains of *S. aureus*. Polyamines, products of arginine metabolism, are made in human tissues, where they participate in basic physiological processes including wound healing and inflammation (19). In a murine skin abscess model, polyamines were shown to contribute to clearance of *S. aureus*, an effect that was mitigated by SpeG, and the ACME *arc* genes appear to drive increased synthesis of polyamines in skin (6).

Polyamines such as spermidine are also known for pleiotropic effects on basic bacterial physiology, including protection from oxidative stress, cell wall formation, and acid tolerance (20). In Gram-negative organisms, including *Vibrio cholerae* (21, 22) and *Yersinia pestis* (23, 24), polyamines are involved in regulation of biofilm formation. In addition, spermidine and spermine toxicity can be synergistic with several classes of antibiotics (25), especially β-lactams, through a mechanism that may involve direct interaction with penicillin binding protein 2 (26).

Since biofilm formation and antibiotic resistance are crucial to *S. aureus* skin colonization, persistence, and transmission, we hypothesized that *speG*-mediated polyamine tolerance would constitute an important adaptation that could explain the remarkable success of USA300 strains. By performing a rigorous phylogenetic analysis of the ACME locus, accompanied by a survey of a diverse collection of clinical isolates, we have provided strong evidence supporting initial assembly of the ACME locus in *S. epidermidis*, and a single, extremely recent horizontal gene transfer to USA300. In addition, we have shown that *speG*-mediated polyamine tolerance allows upregulation of genes required for biofilm formation, increased adherence to abiotic surfaces and fibrinogen/fibronectin, and increased resistance to antibiotics and killing by human keratinocytes. Taken together, these data suggest that acquisition of the *speG* gene was a crucial factor in the evolutionary success of USA300.

RESULTS

The modular ACME was assembled in *S. epidermidis*. To test the hypothesis that ACME was assembled in *S. epidermidis* prior to transfer to USA300, we did an in-depth phylogenetic analysis of representative genes from a diverse collection of draft genomes of *S. epidermidis*. In contrast to the case with *S. aureus*, *S.* epidermidis ACME-related genes were not always found in the same locus, and some genomes lacked certain ACME-related genes entirely (Fig. 1B).

To chart the historical events that led to the assembly of USA300 ACME, we reconstructed gene phylogenies for three genes, *arcA*, *aliD*, and *speG*. Gene trees constructed under maximum-likelihood (ML), maximum-parsimony (MP), and Bayesian criteria had consistent topologies. Based on the incongruence length difference (ILD) test (27), *aliD* and *speG* partitions had congruent historical signals, while *arcA* was significantly different ($P = 0.002$). Tree reconciliation analysis (Fig. 2A) shows that *arcA* may have become newly associated with *speG* genes in three separate events. In one of these events, the *arcA* gene became associated with the *speG-aliD* locus, which was later transferred to USA300 strains.

We predicted that the entire ACME locus would be intact in most strains if it had been transferred in a single event. PCR-based screening of 192 clinical and environmental samples collected in New York City (28) showed that the *speG*, *aliD*, *arcA*, and *opp-3a* genes were never found in isolation from one another, strongly suggesting that the entire ACME locus was present (Fig. 1B; see also Table S1 in the supplemental material). Further screening of a diverse collection of 125 whole-genome sequences revealed only a single instance of a USA300-type ACME gene in isolation (a gene with 98% nucleotide identity to USA300 *speG* from the NRS105 strain).

ACME was transferred to *S. aureus* extremely recently. We next addressed the question of timing, asking when ACME, once assembled, was transferred. To increase phylogenetic resolution and statistical power, we expanded our analysis to include the largest possible segments of ACME loci and focused on the set of ACME loci most closely related to the USA300 lineages. Our phylogeny (Fig. 2B) identified a recent ancestor of the *S. epidermidis* strains VCU050 and NIHLM049 as the likely donor in the horizontal transfer to USA300.

To estimate the timing of the horizontal gene transfer event, we used a Bayesian approach. Using recorded isolation dates localized on the tips of the phylogenetic tree to calibrate divergence times (see Table S2 in the supplemental material), we estimated a median year for the earliest ACME transfer date from *S. epidermidis* to *S. aureus* of 1981 (95% highest posterior density [HPD], 1878 to 1998) (Fig. 2B). Relaxed and strict clock models yielded almost identical dates (see Table S3) and an evolutionary rate of

Downloaded from https://journals.asm.org/journal/mbio on 25 August 2022 by 138.5.97.228.

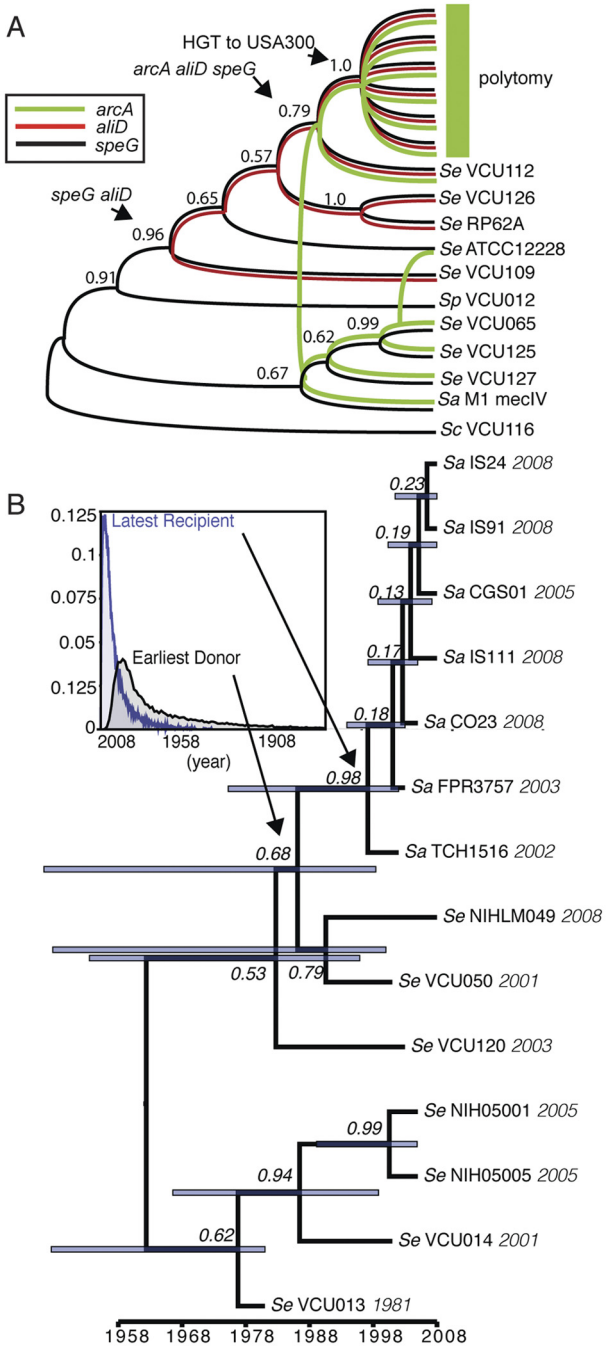

FIG 2 Phylogenetic reconstruction of ACME. (A) Reconciled gene genealogy for *arcA* (green), *aliD* (red), and *speG* (black), which depicts the smallest number of reticulation events based on each gene tree. Numbers on branches are Bayesian clade credibility values for the *speG* locus phylogeny. The polytomy indicated by the green bar represents ACME loci from US300 strains and their very close relatives from *S. epidermidis* and includes all strains found in the tree in panel B. Note that *arcA*, *speG*, and *aliD* coalesced in the same genome just prior to the putative transfer (HGT) to USA300 strains. (B) Bayesian chronogram of ACME loci from the polytomy depicted in panel A, calibrated using the dates of strain isolation. The node bars indicate the uncertainty (95% highest posterior density) for the divergence times. Branch values are the posterior probabilities of clade credibility. (B) Inset shows the distribution of sampled dates for calculation of divergence times from the Bayesian analysis. Abbreviations: *Se*, *S. epidermidis*; *Sa*, *S. aureus*; *Sp*, *Staphylococcus pettenkoferi*; *Sc*, *Staphylococcus capitis*.

$\sim 4.2 \times 10^{-6}$ substitutions/site/year, in agreement with published rates (29, 30). All USA300 ACME loci are estimated to have shared a common ancestor around 1997 (95% HPD, 1975 to 2001). Therefore, it is likely that the transfer of ACME occurred between 1981 and 1997, just prior to the expansion of USA300.

Polyamines enhance *S. aureus* USA300 biofilm formation when *speG* is present. The *speG* locus appears to have been added to the rest of the ACME locus in the steps leading up to its successful horizontal transfer into *S. aureus*. Thus, we hypothesized that *speG* may be the crucial factor that gives USA300 strains a selective advantage. Alleviation of spermidine/spermine toxicity may have been an important adaptation, since close relatives of USA300 that lack ACME, and thus the *speG* gene, are highly susceptible to spermidine killing (see Fig. S1 in the supplemental material).

We predicted that other beneficial traits associated with the ability to survive polyamine challenge might also have had an impact. To test whether or not spermidine would enhance biofilm formation as it does in Gram-negative organisms (21–24), *S. aureus* USA300 was grown in various concentrations of spermidine chosen to reflect physiologic levels present in skin and wounds (6, 31). Biofilm formation was quantified using a standard crystal violet (CV) assay. Treatment with spermidine elicited a dose-dependent increase in biofilm formation and the development of characteristic mound or mushroom-like structures (Fig. 3).

The largest increases in biofilm formation occur at spermidine levels that are toxic to ACME-minus strains (Fig 3; see also Fig S1 in the supplemental material). Comparison of wild-type USA300 and the isogenic *speG* null mutant showed a similar result, and complementation of the *speG* null strain with the wild-type *speG* gene in *trans* restored the ability to survive and form increased biofilms (Fig. 3D, E, and F). We observed small increases in biofilm in both *speG*-positive and -negative strains exposed to sublethal (5.75 mM) doses of spermidine (Fig. 3D to F). These results were similar with spermine, but putrescine had no obvious effect on biofilms or viability (Fig. 3F; see also Fig. S2 in the supplemental material).

Spermidine/spermine significantly increase pH when they are added to media, and it is known that polyamine toxicity is pH dependent (see Fig. S2) (18). To explore the impact of pH on biofilm formation, we compared bacteria grown in the presence of spermidine to those grown in medium adjusted to the same pH values (Fig. 4A). Exposure to spermidine caused significantly more biofilm formation than pH-matched medium, suggesting that increased biofilm formation cannot be explained by alkaline stress alone. In contrast, *N*-acetylspermidine had no impact on biofilm formation at any pH (Fig. 4A; see also Fig. S2), which also suggests that the predicted product of the SpeG acetyltransferase reaction is not involved in biofilm formation.

Spermidine-induced biofilms appear to be structurally similar to other *S. aureus* biofilms. They are susceptible to disruption with agents that target proteins and extracellular DNA (eDNA) (Fig. 4B and C), but they are not disrupted by the addition of dispersin B, an enzyme that targets biofilm-associated polysaccharide (polysaccharide intercellular antigen [PIA]/poly-*N*-acetylglucosamine [PNAG]) (32) (Fig. 4D).

Spermidine increases transcription of biofilm genes. *S. aureus* biofilm formation is regulated by the *agr* quorum-sensing regulatory system, with repression of *agr* leading to increased biofilm formation (33–36). We used quantitative reverse transcription-PCR (qRT-PCR) to assess whether or not

Downloaded from https://journals.asm.org/journal/mbio on 25 August 2022 by 138.5.97.228.

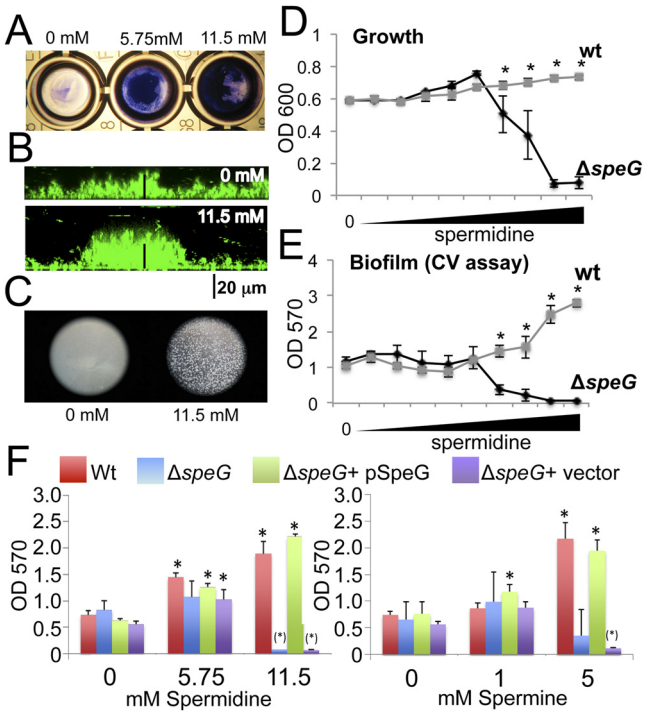

FIG 3 Biofilm formation in the presence of spermidine. (A) Crystal violet (CV)-stained biofilms formed after exposure of wild-type USA300 to spermidine. (B) Confocal imaging of wild-type USA300 expressing GFP, grown with and without spermidine. Note the formation of larger dome-shaped structures in the spermidine-exposed bacteria. The black bar shows the scale (20 μm). (C) Grossly visible clumping/autoaggregation of strains exposed to spermidine (magnification, ×40). (D and E) Growth (18 h, 37°C, in TSB with 0.4% glucose) and biofilm formation, respectively, in various concentrations of spermidine (0, 0.35, 0.7, 1.4, 2.8, 5.6, 6.5, 7.5, 9.4, and 11.5 mM) for wild-type (wt) and Δ*speG* strains. Major increases in biofilm formation occur at levels of spermidine that are lethal to the Δ*speG* strain. Data were analyzed with a one-way ANOVA. "*" indicates $P < 0.001$ for a Bonferroni posttest comparing the wild type to the Δ*speG* strain. (F) Biofilm formation as quantified by a CV assay for the wild-type USA300 strain compared with isogenic Δ*speG* mutant strains at various concentrations of spermidine (0 mM, 5.75 mM, and 11.5 mM) and spermine (0 mM, 1 mM, and 5 mM). The complemented (Δ*speG* + pSpeG) and vector control (Δ*speG* + vector) strains are also shown. Data shown constitute a single representative of the experiment, which was replicated in quintuplicate. A one-way ANOVA test was performed for each strain, comparing each of the three concentrations for each polyamine. Asterisks indicate a Dunnett's posttest result of $P < 0.01$ when comparing each value with that for the no-spermidine control for each strain. Note that asterisks in parentheses denote values for severely attenuated growth and are therefore not due to decreased biofilm formation.

spermidine-induced biofilms had the expected changes in *agr* expression (Fig. 5A). Indeed, cultures exposed to spermidine showed a rapid reduction of *agrC* expression over a 3-h time course. The cell wall-associated adhesin fibronectin binding protein A (encoded by *fnbA*), which has been shown to be involved in biofilm formation (37), was increased in expression. The *cidA* gene, which enhances biofilm formation through production of eDNA (38), and the *icaA* gene, which is involved in production of the biofilm-associated PIA (39), were also upregulated. The *atl* gene, which encodes a protein (autolysin) involved in early stages of the FnbA-mediated biofilm phenotype (40), was upregulated within the first 30 min of exposure to spermidine.

Spermidine enhances binding to fibronectin and fibrinogen. The cell wall-associated adhesins ClfA and FnbA bind to the matrix components, such as fibrinogen (41, 42) and fibronectin (43), that are important in the pathogenesis of skin infection. Because spermidine increased expression of the genes *clfA* and *fnbA* (Fig. 5A), we hypothesized that it would also enhance binding to these substrates. Using a chemiluminescence assay, we found that addition of spermidine enhanced adherence of *S. aureus* to fibrinogen and fibronectin in a dose-dependent manner (Fig. 5B).

***fnbA* and *fnbB* are required for the full spermidine-enhanced biofilm phenotype.** A preliminary assay of *fnbA* and *fnbB* insertion mutants (NARSA-Nebraska Library) showed significant deficits in spermidine-enhanced biofilm formation (data not shown). A USA300 LAC Δ*fnbAB* mutant showed an overall reduction in biofilm biomass and a significant proportional (2-fold) decrease ($P < 0.0001$) in the ability of spermidine to enhance biofilm formation (Fig. 5C). The complete extent of biofilm formation was restored with complementation in *trans* with either *fnbA* or *fnbB*. Of note, additional spermidine-enhanced biofilm formation was observed in the mutant and in complemented mutant strains, suggesting that the phenotype is multifactorial.

***speG* contributes to antimicrobial resistance.** There is documented synergy between the toxic effects of spermidine and several antibiotics (25), most notably β-lactams (26). We hypothesized that such synergy would be disrupted by the presence of the *speG* gene. We assayed MICs using an Etest-based approach with sublethal concentrations of spermidine added to solid medium (Fig. 5A). We observed a striking decrease in synergy between spermidine and oxacillin for the wild type compared to that for *speG* mutant. There were also significant decreases in synergy with clindamycin, gentamicin, and mupirocin, all of which are important antibiotics for treatment of staphylococcal infection (Fig. 5B). There were no significant changes in MIC for other antistaphylococcal antibiotics, such as daptomycin, vancomycin, and trimethoprim-sulfamethoxazole. For doxycycline, we observed an antagonistic effect, and we noted a protective effect for tetracycline, consistent with findings of other studies (see Fig. S4 in the supplemental material) (44). The mechanism of this antagonistic effect is not well understood, but it may be due to spermidine's ability to protect against oxygen radicals (44).

***speG* ameliorates spermidine-enhanced killing by human keratinocytes.** Human keratinocytes have antistaphylococcus activity that is thought to be due to the action of several antimicrobial peptides (45, 46), especially human β–defensin 3 (hBD3) (47). By analogy with the observed antibiotic effects, we hypothesized that spermidine may potentiate keratinocyte killing. Indeed, in the presence of keratinocytes, the MIC of spermidine was greatly reduced for both wild-type and *speG* null strains (Fig. 6B and C). This effect was more pronounced in the *speG* null strain, which was killed even at a 10th of the MIC of medium alone, providing further evidence for an *in vivo* selective advantage of *speG*-positive strains.

DISCUSSION

Large increases in hospitalizations for severe skin infections from 2000 to 2009 (48) coincide with the geographic spread of the USA300 MRSA clone (1) and its replacement of other *S. aureus* strains as the most common cause of skin and soft-tissue infections (2, 4). Such epidemiological observations suggest that there was a major evolutionary event or series of events that changed the biology of USA300 strains, making them more fit, transmissible, and potentially more virulent. Here we explored one possible con-

Downloaded from https://journals.asm.org/journal/mbio on 25 August 2022 by 138.5.97.228.

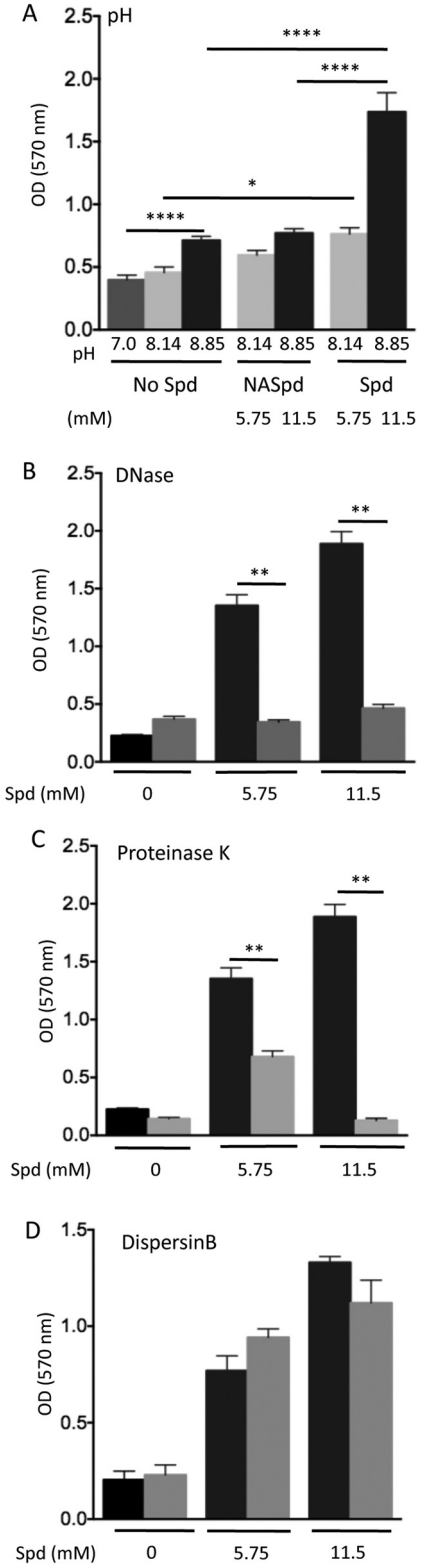

FIG 4 Properties of the spermidine-enhanced biofilm. (A) Effect of initial pH on biofilm formation by wild-type USA300. Strains were grown either in the presence of spermidine (Spd) (0 mM, 5.75 mM, or 11.5 mM) or in culture medium with matching pH titrated by addition of NaOH (light gray, pH 8.14; black, pH 8.85). Biofilms were measured using the crystal violet assay. Histograms show a single representative result from one experimental replicate. All experiments were repeated three times. A one-way ANOVA with Tukey's post-

(Continued)

tribution to this rapid epidemiological and geographic expansion, the acquisition of the ACME locus.

Phylogenetic analysis shows that the genes of the USA300 ACME locus coalesced into a single genetic locus prior to a single transfer into *S. aureus* USA300. Given the strong association with methicillin resistance in clinical strains, it is likely that the recipient had already acquired the *mec* type IV element. Our Bayesian analysis suggests that the acquisition of ACME in USA300 most likely occurred between 1981 and 1997, temporally linking this event to the expansion of this clone.

There are now multiple reports of diverse ACME regions in non-USA300 strains that are characterized by presence of the *arc* operon but are otherwise genetically distinct (11–14). In particular, the association of the *speG* locus with other ACME genes appears to be very uncommon outside of USA300. Addition of the *speG* gene to ACME may have been a key step in the successful horizontal transfer to USA300 strains. Spermidine is produced especially in areas of keratinocyte proliferation, inflammation, and wound healing (19), conditions under which *S. aureus* invades and causes skin infection. Polyamines may be further increased in the presence of ACME genes (6). One explanation for increased fitness is that the product of *speG* simply neutralizes the toxic effects of spermidine produced in human skin (6, 18), but the other spermidine-associated traits demonstrated in this report could also significantly enhance effective colonization, transmission, and infection.

Biofilm formation is thought to be a critical bacterial strategy for colonization and infection of skin (49). We showed here that *S. aureus* demonstrates strong increases in biofilm formation in the presence of polyamines, likely due to upregulation of genes involved in adherence and biofilm formation. In particular, we showed that expression of the genes encoding fibronectin binding proteins (*fnbA* and *fnbB*) is required for the full spermidine-induced biofilm phenotype. However, increases in biofilm formation even in the absence of *fnbA* and *fnbB* suggest that the effect of spermidine on biofilm formation is multifactorial. This effect may include the contribution of other biofilm proteins or genes involved in production of extracellular DNA (eDNA). In addition, spermidine is known to bind and stabilize nucleic acids, which could stabilize the eDNA structural component of biofilms. Recent evidence has also indicated that norspermidine may be involved in staphylococcal biofilm disassembly through direct interactions with exopolysaccharide (50), raising the possibility that spermidine interacts directly with exopolysaccharide to competitively inhibit dispersal. However, our dispersal data suggest that polysaccharide (PIA/PNAG) is not an important component of spermidine-enhanced biofilms.

Genes upregulated in response to spermidine (i.e., *fnbA* and *clfA*) are critical for adherence to the host extracellular matrix

Figure Legend Continued

test was used for analysis. *, $P < 0.05$; ****, $P < 0.0001$. NASpd, *N*-acetylspermidine. (B to D) Effect of proteinase K (10 μg/ml) (B), DNase (2 μg/ml) (C), or dispersin B (10 μg/ml) (D) on wild-type USA300 after growth in various concentrations of spermidine (0 mM, 5.75 mM, and 11.5 mM). Biofilms formed overnight were treated (gray) with proteinase K, DNase, or dispersin B for 1 h and then measured with the CV assay. One-way ANOVA was used to analyze data at each spermidine concentration. **, $P < 0.01$ after Dunnett's posttest comparing each treatment value with that for the untreated control (black).

Downloaded from https://journals.asm.org/journal/mbio on 25 August 2022 by 138.5.97.228.

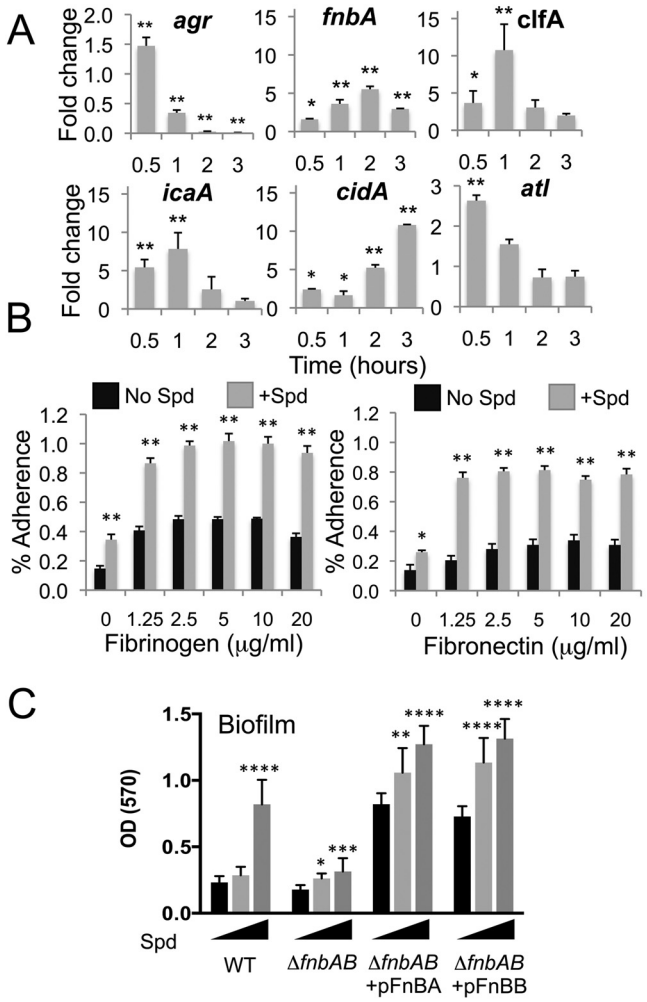

FIG 5 Biofilm and adhesin genes in spermidine-enhanced biofilms. (A) Wild-type USA300 was grown in broth with or without spermidine (11.5 mM) for 0.5, 1, 2, and 3 h, and mRNA levels were analyzed by qRT-PCR (see Materials and Methods). Relative quantification (RQ) fold difference values from triplicate readings in one representative experiment with standard deviations are shown. The experiment was replicated in triplicate. Results are expressed as the ratio of mRNA transcript (pmol/vol) between spermidine-exposed and -unexposed bacteria at each time point. A one-way ANOVA test was used to analyze the data. **, $P < 0.001$; *, $P < 0.05$ after a Bonferroni posttest comparing exposed to unexposed samples at each time point). (B) Wild-type USA300 adherence to fibronectin/fibrinogen (0, 1.25, 2.5, 5, 10, or 20 μg/ml)-coated plates. BacTiter-Glo luminescence was used to quantify the proportion of adherent bacteria. Values represent proportions of luminescence measured when wells were washed to total luminescence in the entire well. One-way ANOVA was used to analyze these data. **, $P < 0.001$; *, $P < 0.05$ (after a Bonferroni posttest comparing exposed to unexposed samples at each fibrinogen/fibronectin concentration). (C) Crystal violet (CV) biofilm assay; results for the fibronectin binding protein double mutant (Δ*fnbAB*) and complemented mutants expressing either *fnbA* or *fnbB* in *trans* are compared to those for the isogenic wild-type strain with biofilms grown with 0 mM (black), 5.75 mM (light gray), or 11.5 mM (dark gray) of spermidine. Results show one representative experiment. The experiment was repeated in triplicate. A one-way ANOVA test was used to analyze these data. ****, $P < 0.0001$; ***, $P < 0.001$; **, $P < 0.01$; and *, $P < 0.05$ after Dunnett's posttest for each strain compared to the 0 mM spermidine condition.

proteins fibrinogen and fibronectin. Keratinocytes and skin fibroblasts produce fibronectin, which is abundant in the skin (51) and along with fibrinogen is important in clot formation and wound healing (51, 52). SpeG-enhanced binding of *S. aureus* to these substrates could facilitate the initial steps of wound infection. The interaction between the FnbA adhesin and fibronectin is also required for integrin-mediated intracellular invasion of keratinocytes (53).

In the era of widespread antibiotic use, synergy between polyamines and antibiotics (25) likely constitutes a major selective pressure and may be especially relevant in skin, where there are relatively large concentrations of polyamines (31). The presence of *speG* not only ameliorates the toxicity of spermidine at high doses but also enhances bacterial survival in the presence of antibiotics at sublethal doses (Fig. 6). The robust synergy with oxacillin suggests that a major advantage of the presence of *speG* may be enhancement of the methicillin resistance phenotype. Notably, there is also synergy with mupirocin, a topical antibiotic that is widely used with the aim of eradicating MRSA colonization.

The acquisition of *speG* may have made USA300 strains less prone to killing by the innate defenses of human keratinocytes. Exogenous spermidine, even at low concentrations, greatly enhanced killing of wild-type USA300 by human keratinocytes. For the *speG* mutant, this effect was even more pronounced with significant killing at every concentration of spermidine we tested. Although the mechanism behind this killing is not clear, it is possible that spermidine synergizes with antimicrobial peptides produced by keratinocytes.

There were undoubtedly multiple biological events that led to the rapid population expansion and replacement of other *S. aureus* strains by the USA300 community-associated MRSA (CA-MRSA) clone. Changes in expression levels of key virulence genes (e.g., those encoding phenol soluble modulins and alpha-toxin) likely had a major impact on the virulence of this strain (54, 55). However, virulence is not the only factor in the evolutionary success of a pathogen. Key adaptations may have occurred in colonization, persistence, and transmissibility.

Our phylogenetic and microbiological data lead us to propose the following scenario. Genomic rearrangement and recombination led to the positioning of the *speG* locus immediately adjacent to the rest of ACME in an ancestral *S. epidermidis* strain. Because of the physical proximity of *speG* to the *arc* genes, a single horizontal transfer event of the entire region resulted in acquisition of a detoxification gene (*speG*), along with a system that increases production of the toxic metabolite (*arc*) in human skin, ensuring the stability of the entire locus in the recipient. The acquisition of *speG* also had other important *positive* benefits for the recipient USA300 strain. Polyamine tolerance led to enhanced biofilm formation and adherence, decreased antibiotic susceptibility, and decreased killing by human keratinocytes. All of these properties would be key adaptations that enhanced colonization and persistence on human skin, perhaps leading to more effective spread and a competitive advantage over other strains.

MATERIALS AND METHODS

Phylogenetic and sequence analysis for tree reconciliation. Nucleotide sequences for *speG* (GenBank accession no. YP_492772.1), *aliD* (accession no. ABD22386.1), and *arcA* (accession no. YP_492784.1) were used as queries in searching of public databases and genomic data from genome drafts of strains from the NARSA *S. aureus* and *S. epidermidis* genome sequencing project (courtesy of G. Archer and B. Kreiswirth). Codon-based alignments were done using the MUSCLE algorithm (56) in the software program MEGA (57) with default parameters (see Data Set S1 in

Downloaded from https://journals.asm.org/journal/mbio on 25 August 2022 by 138.5.97.228.

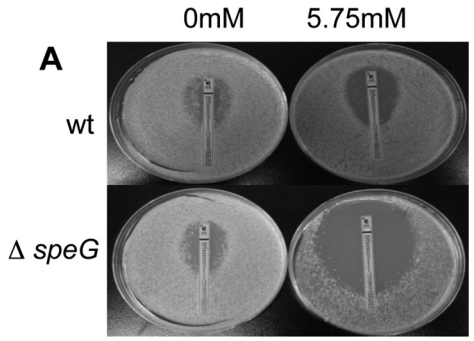

B

Spermidine	MIC of USA300 (μg/ml) 0mM ΔspeG	5.75mM ΔspeG	0mM wt	5.75mM wt
Ciprofloxacin	0.25	1	0.25	0.38
Clindamycin	0.19	≤0.016*	0.19	0.064
Daptomycin	4	2*	3	3
Doxycycline	1	1	1	4
Gentamicin	1.5	0.19	1	0.38
Mupirocin	0.38	0.19*	0.75	1
Oxacillin	4	0.064*	4	1.5
Polymixin	64	1*	48	12
Trimethoprim sulfamethoxazole	0.125	0.19	0.19	0.125
Vancomycin	3	4	2.5	4

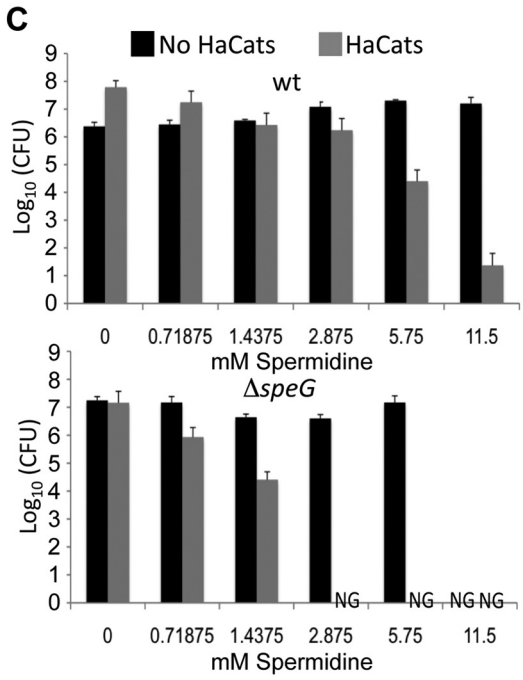

FIG 6 Spermidine synergy with antibiotics and human keratinocytes. (A) Oxacillin Etest on solid agar in the presence or absence of spermidine at 5.75 mM. Note that changes in both halo diameter and the point of intersection with the strip show less synergy between oxacillin and spermidine when *speG* is present. (B) Table of the Etest MIC data for other important anti-staphylococcal antibiotics. All Etest values were determined in triplicate. Light-gray cells denote MIC changes of 2 dilutions with addition of spermidine, darker gray cells indicate MIC changes of more than 2 dilutions. An asterisk denotes a change in the maximum halo diameter of more than 50%. (C) Shown are growth/survival at different concentrations of spermidine for *(Continued)*

the supplemental material). We used the program PAUP 4b10 (2003; Sinauer, Sunderland, MA) for MP analyses and the incongruence-length difference (ILD) analysis (see Data Set S1), the program MrBayes 3.1.2 (58) for Bayesian Markov chain Monte Carlo (MCMC) analysis, and the RAxML 7.4.1 program (59) for ML analysis. For tree reconciliation, we reconciled trees both by hand and using the software program TreeMap 3 (https://sites.google.com/site/cophylogeny/), assigning duplications and losses equal weight, and solving for the minimum sum of these events.

Bayesian estimation of the timing of the ACME horizontal event. For resolving close phylogenetic relationships and estimating divergence times, we used draft assemblies of *S. epidermidis* genomes from the *S. epidermidis* genome sequencing projects. We completed assembly of contiguous ACME loci using genomic DNA from close *S. epidermidis* strains for PCR and Sanger sequencing. We aligned ACME loci with default parameters of MUSCLE (56) in two sections corresponding to the *speG* and *arc-opp* gene loci, respectively (total = 14 taxa and 21.3 kb) (see Data Set S1 in the supplemental material). We used the date of strain isolation to calibrate coestimation of the phylogeny and divergence times in the software program BEAST 1.7.4 (60) using the general time-reversible nucleotide substitution model with among-site rate heterogeneity, with the Γ distribution and four discrete rate categories (GTR plus Γ_4). Evolutionary rates across the phylogenetic tree were allowed to vary using the uncorrelated lognormal relaxed-clock model (61) as well as a strict clock and a uniform prior on the overall evolutionary rate in the range 10^{-7} to 10^{-5} substitutions × site^{-1} × year^{-1} (29, 30). The Markov chain Monte Carlo procedure was run five times for 100 million generations, sampling every 5,000 steps. Convergence was assessed by observing the expected sample size (ESS) values (>200) and by inspecting the LogLikelihood trace. The relaxed and strict models were compared using Bayes factors.

Bacterial strains and cultures. *S. aureus* strains SF8300 (USA300 wild type), AR0417 (Δ*speG* derivative of SF8300), ARO581 (AR0417 with the pLZ12-Sp-speG complementing plasmid), and AR0582 (AR0417 with the pLZ12-Sp vector) were provided by A. Richardson (18). *S. aureus* strain SA108 is a derivative of USA300 FPR3757 expressing green fluorescent protein (GFP) from the pCU1(Cm^r) shuttle vector. *S. aureus* LAC strains, including the Δ*fnbAB* strain and its isogenic parent, and mutants with complementing plasmids [pFnBA4(Cm^r) and pFnBB4(Cm^r)] were provided by J. Geoghegan (62). *S. epidermidis* strains VCU013, VCU014, VCU050, VCU112, and VCU120 were provided by G. Archer. In general, strains were plated on trypticase soy agar (TSA) and grown overnight at 37°C. Single colonies were inoculated in tryptic soy broth (TSB) and grown overnight with shaking at 37°C. Strains ARO581 and AR0582 were grown with spectinomycin (100 μg/ml), and SA108 and the complemented Δ*fnbAB* mutant were grown in chloramphenicol (10 μg/ml), to ensure plasmid stability. Clinical samples of *S. aureus* were provided from the collection of F. Lowy and A. C. Uhlemann. *S. aureus* strains were collected as part of a prior study in New York City, NY, between January 2009 and May 2010 (28) (IRB AAAD0052; Columbia University).

PCR and BLAST-based screening. The presence of *arcA* and *opp3AB*, *spa*-type clonal complex, pulse field gel electrophoresis (PFGE), and *mec* type were determined previously (28). PCR primers to *speG* and *aliD* were used to screen 192 clinical isolates using PCR (see Text S1 in the supplemental material). We performed *in silico* screening of whole genomes and genome drafts using the BLASTn application (default parameters), using the *arcA*, *aliD*, and *speG* USA300 genes as queries. *S. aureus* genomes were scored as having ACME-type versions of each of the genes if the ranked bit score was equivalent to or higher than the best hit from any *S. epidermidis* strain. Likewise, *S. epidermidis* genomes were scored as having each of the

Figure Legend Continued

wild-type USA300 or the isogenic Δ*speG* mutant after 24 h of culture on a confluent layer of human keratinocytes (HaCats). Black bars show growth in HaCat medium without keratinocytes. One-way ANOVA *P* values were 0.0364 and 0.0038 for the Δ*speG* strain and the wild type, respectively.

Downloaded from https://journals.asm.org/journal/mbio on 25 August 2022 by 138.5.97.228.

genes if there was a hit for which the bit score was equivalent to or higher than that for the best non-USA300 *S. aureus* strain.

Biofilm formation. For all biofilm formation assays, strains were grown overnight statically at 37°C in TSB with an additional 0.4% glucose. Biofilm formation was quantified using a standard crystal violet biomass assay (see Text S1 in the supplemental material). For dispersal assays, DNase I (10 μg/ml), proteinase K (2 μg/ml) (Sigma-Aldrich), or dispersin B (10 μg/ml) (Kane, Biotech) was added to wells after 24 h of static biofilm formation and incubated for 1 h at 37°C prior to the crystal violet assay.

Confocal microscopy. *S. aureus* USA300 strain FPR3757 expressing GFP from the pCU1 plasmid was grown overnight under biofilm-forming conditions (TSB with 0.4% glucose with or without spermidine at 11.5 mM) with 10 μg/ml chloramphenicol in coverglass chamber slides. Slides were washed with PBS and then fixed in 4% paraformaldehyde for 10 min. Bacteria were imaged using a Zeiss LSM 510 Meta scanning confocal microscope with a Plan-Neofluar 100×/1.3 oil objective at room temperature. Image acquisition and presentation were performed using LSM Image Browser 4.2 software (Zeiss).

Transcriptional activation of biofilm genes. Overnight culture of the wild-type strain was diluted and grown with shaking at 37°C to an optical density at 600 nm (OD_{600}) of 1.0. Bacteria were washed and resuspended with or without 11.5 spermidine mM in TSB 0.4% Glucose, and aliquoted (200 μl/well) in sterile 96-well flat-bottom plates (CytoOne). Plates were incubated at 37°C, and samples were collected at 30 min, 1 h, 2 h, and 3 h. RNA preparation and qRT-PCR was performed as described previously (63) (see Text S1 in the supplemental material).

Fibronectin/fibrinogen binding assay. Human fibronectin and fibrinogen in Dulbecco's phosphate-buffered saline (D-PBS) diluted to specified concentrations (20, 10, 5, 2.5, and 1.25 μg/ml) was used to coat 96-well flat-bottom enzyme-linked immunosorbent assay (ELISA) plates overnight at 4°C. Wells were washed with PBS–0.05% Tween 20 (washing buffer [WB]), blocked for 1 h at room temperature with WB plus 1% bovine serum albumin, and then washed again with WB. Strains were grown to an OD_{600} of 1.0 and then washed, resuspended to an OD_{600} of 0.450 in TSB–0.4% glucose with or without 11.5 mM spermidine, and inoculated into wells. After a 1-h incubation at 37°C, the supernatant was removed and wells were washed aggressively with WB to remove nonadherent bacteria. We then added 50 μl of BacTiter-Glo microbial cell viability luminescence (Promega) mixture to each well, and luminescence was detected on a Tecan I-Control plate reader. Data were interpreted as the amount of bacteria bound after washing divided by the amount of total bacteria compared to findings for unwashed wells.

Antibiotic and polyamine MIC test. Strains were grown overnight and then to an OD_{600} to 1.0. One hundred microliters of each strain was plated on TSA with or without 5.75 mM spermidine. Antibiotic Etest strips (bioMérieux) for each antibiotic were placed on the plated bacteria and incubated at 37°C overnight. The MIC was determined at the intersection of the inhibitory halo with the strip.

HaCat killing assay. Human keratinocytes (HaCats) were grown to confluence (10 days) in RPMI medium 1640 with 10% fetal bovine serum (FBS). Twenty-four hours prior to bacterial exposure, the HaCat medium was changed to antibiotic and FBS-free medium. After 24 h, HaCats were washed three times in PBS to remove any remaining antibiotic and then incubated in RPMI medium 1640 with fibronectin (1 μg/ml) for 1 h. Spermidine was added in appropriate concentrations, along with 10 μl of bacterial culture (OD_{600} of 1.0). After static incubation overnight at 37°C, supernatant CFUs were determined. CFUs were also determined from vigorous disruption of adherent cells using an additional step of treatment with the Triple Express reagent (Gibco) at 37°C with 5% CO_2 for 60 min followed by sterile scraping scraped of the bottom of each well.

Statistical analysis. All statistical analyses were done using the software program Prism (GraphPad). Multiple comparisons were analyzed using one-way analysis of variance (ANOVA) with appropriate posttest as detailed in the figure legends.

SUPPLEMENTAL MATERIAL

Supplemental material for this article may be found at http://mbio.asm.org/lookup/suppl/doi:10.1128/mBio.00889-13/-/DCSupplemental.

Text S1, DOCX file, 0.2 MB.
Figure S1, PDF file, 0.1 MB.
Figure S2, PDF file, 0.1 MB.
Figure S3, PDF file, 0.1 MB.
Figure S4, PDF file, 0.1 MB.
Table S1, DOCX file, 0.1 MB.
Table S2, DOCX file, 0.1 MB.
Table S3, DOCX file, 0.1 MB.
Data Set S1, TXT file, 0.6 MB.

ACKNOWLEDGMENTS

This work was supported by grants to P.J.P. (UL1 TR000040) and A.S.P. (NIH R01 HL079395 and NIH RO1 AI 103854).

We thank Barry Kreiswirth and Gordon Archer for early access to *S. aureus* and *S. epidermidis* draft genome data. We thank Julie Segre, Garth Ehrlich, Binh Diep, and Sarah Highlander for isolation date information on staphylococci.

REFERENCES

1. **Tenover FC, Goering RV.** 2009. Methicillin-resistant *Staphylococcus aureus* strain USA300: origin and epidemiology. J. Antimicrob. Chemother. **64:**441–446.
2. **Moran GJ, Krishnadasan A, Gorwitz RJ, Fosheim GE, McDougal LK, Carey RB, Talan DA, Net, EMERGEncy ID Study Group.** 2006. Methicillin-resistant *S. aureus* infections among patients in the emergency department. N. Engl. J. Med. **355:**666–674. doi:10.1056/NEJMoa055356.
3. **Seybold U, Kourbatova EV, Johnson JG, Halvosa SJ, Wang YF, King MD, Ray SM, Blumberg HM.** 2006. Emergence of community-associated methicillin-resistant *Staphylococcus aureus* USA300 genotype as a major cause of health care-associated blood stream infections. Clin. Infect. Dis. **42:**647–656.
4. **Klevens RM, Morrison MA, Nadle J, Petit S, Gershman K, Ray S, Harrison LH, Lynfield R, Dumyati G, Townes JM, Craig AS, Zell ER, Fosheim GE, McDougal LK, Carey RB, Fridkin SK, Active Bacterial Core surveillance (ABCs) MRSA Investigators.** 2007. Invasive methicillin-resistant *Staphylococcus aureus* infections in the United States. JAMA **298:**1763–1771.
5. **Otto M.** 2011. A MRSA-terious enemy among us: end of the PVL controversy? Nat. Med. **17:**169–170.
6. **Thurlow LR, Joshi GS, Clark JR, Spontak JS, Neely CJ, Maile R, Richardson AR.** 2013. Functional modularity of the arginine catabolic mobile element contributes to the success of USA300 methicillin-resistant *Staphylococcus aureus*. Cell Host Microbe **13:**100–107.
7. **Barbier F, Lebeaux D, Hernandez D, Delannoy AS, Caro V, François P, Schrenzel J, Ruppé E, Gaillard K, Wolff M, Brisse S, Andremont A, Ruimy R.** 2011. High prevalence of the arginine catabolic mobile element in carriage isolates of methicillin-resistant *Staphylococcus epidermidis*. J. Antimicrob. Chemother. **66:**29–36.
8. **Diep BA, Gill SR, Chang RF, Phan TH, Chen JH, Davidson MG, Lin F, Lin J, Carleton HA, Mongodin EF, Sensabaugh GF, Perdreau-Remington F.** 2006. Complete genome sequence of USA300, an epidemic clone of community-acquired meticillin-resistant *Staphylococcus aureus*. Lancet **367:**731–739.
9. **Miragaia M, de Lencastre H, Perdreau-Remington F, Chambers HF, Higashi J, Sullam PM, Lin J, Wong KI, King KA, Otto M, Sensabaugh GF, Diep BA.** 2009. Genetic diversity of arginine catabolic mobile element in *Staphylococcus epidermidis*. PLoS One **4:**e7722. doi:10.1371/journal.pone.0007722.
10. **Pi B, Yu M, Chen Y, Yu Y, Li L.** 2009. Distribution of the ACME-arcA gene among meticillin-resistant *Staphylococcus haemolyticus* and identification of a novel ccr allotype in ACME-arcA-positive isolates. J. Med. Microbiol. **58:**731–736.
11. **Goering RV, McDougal LK, Fosheim GE, Bonnstetter KK, Wolter DJ, Tenover FC.** 2007. Epidemiologic distribution of the arginine catabolic mobile element among selected methicillin-resistant and methicillin-susceptible *Staphylococcus aureus* isolates. J. Clin. Microbiol. **45:**1981–1984.

Downloaded from https://journals.asm.org/journal/mbio on 25 August 2022 by 138.5.97.228.

12. **Sabat AJ, Kock R, Akkerboom V, Hendrix R, Skov RL, Becker K, Friedrich AW.** 2013. Novel organization of arginine catabolic mobile element and staphylococcal cassette chromosome *mec* composite island and its horizontal transfer between distinct *Staphylococcus aureus* genotypes. Antimicrob. Agents Chemother. **57:**5774–5777.
13. **Shore AC, Rossney AS, Brennan OM, Kinnevey PM, Humphreys H, Sullivan DJ, Goering RV, Ehricht R, Monecke S, Coleman DC.** 2011. Characterization of a novel arginine catabolic mobile element (ACME) and staphylococcal chromosomal cassette mec composite island with significant homology to *Staphylococcus epidermidis* ACME type II in methicillin-resistant *Staphylococcus aureus* genotype ST22-MRSA-IV. Antimicrob. Agents Chemother. **55:**1896–1905.
14. **Urushibara N, Kawaguchiya M, Kobayashi N.** 2012. Two novel arginine catabolic mobile elements and staphylococcal chromosome cassette mec composite islands in community-acquired methicillin-resistant *Staphylococcus aureus* genotypes ST5-MRSA-V and ST5-MRSA-II. J. Antimicrob. Chemother. **67:**1828–1834.
15. **Wang CH, Lin CY, Luo YH, Tsai PJ, Lin YS, Lin MT, Chuang WJ, Liu CC, Wu JJ.** 2005. Effects of oligopeptide permease in group a streptococcal infection. Infect. Immun. **73:**2881–2890.
16. **Diep BA, Stone GG, Basuino L, Graber CJ, Miller A, des Etages SA, Jones A, Palazzolo-Ballance AM, Perdreau-Remington F, Sensabaugh GF, DeLeo FR, Chambers HF.** 2008. The arginine catabolic mobile element and staphylococcal chromosomal cassette mec linkage: convergence of virulence and resistance in the USA300 clone of methicillin-resistant *Staphylococcus aureus*. J. Infect. Dis. **197:**1523–1530.
17. **Montgomery CP, Boyle-Vavra S, Daum RS.** 2009. The arginine catabolic mobile element is not associated with enhanced virulence in experimental invasive disease caused by the community-associated methicillin-resistant *Staphylococcus aureus* USA300 genetic background. Infect. Immun. **77:**2650–2656.
18. **Joshi GS, Spontak JS, Klapper DG, Richardson AR.** 2011. Arginine catabolic mobile element encoded speG abrogates the unique hypersensitivity of *Staphylococcus aureus* to exogenous polyamines. Mol. Microbiol. **82:**9–20.
19. **Seiler N, Atanassov CL.** 1994. The natural polyamines and the immune system. Prog. Drug Res. **43:**87–141.
20. **Wortham BW, Patel CN, Oliveira MA.** 2007. Polyamines in bacteria: pleiotropic effects yet specific mechanisms. Adv. Exp. Med. Biol. **603:**106–115.
21. **Lee J, Sperandio V, Frantz DE, Longgood J, Camilli A, Phillips MA, Michael AJ.** 2009. An alternative polyamine biosynthetic pathway is widespread in bacteria and essential for biofilm formation in *Vibrio cholerae*. J. Biol. Chem. **284:**9899–9907.
22. **McGinnis MW, Parker ZM, Walter NE, Rutkovsky AC, Cartaya-Marin C, Karatan E.** 2009. Spermidine regulates *Vibrio cholerae* biofilm formation via transport and signaling pathways. FEMS Microbiol. Lett. **299:**166–174.
23. **Patel CN, Wortham BW, Lines JL, Fetherston JD, Perry RD, Oliveira MA.** 2006. Polyamines are essential for the formation of plague biofilm. J. Bacteriol. **188:**2355–2363.
24. **Wortham BW, Oliveira MA, Fetherston JD, Perry RD.** 2010. Polyamines are required for the expression of key Hms proteins important for Yersinia pestis biofilm formation. Environ. Microbiol. **12:**2034–2047.
25. **Kwon DH, Lu CD.** 2007. Polyamine effects on antibiotic susceptibility in bacteria. Antimicrob. Agents Chemother. **51:**2070–2077.
26. **Yao X, Lu CD.** 2012. A PBP 2 mutant devoid of the transpeptidase domain abolishes spermine-beta-lactam synergy in *Staphylococcus aureus* Mu50. Antimicrob. Agents Chemother. **56:**83–91.
27. **Farris JS, Kallersjo M, Kluge AG, Bult C.** 1995. Constructing a significance test for incongruence. Syst. Biol. **44:**570–572.
28. **Uhlemann AC, Knox J, Miller M, Hafer C, Vasquez G, Ryan M, Vavagiakis P, Shi Q, Lowy FD.** 2011. The environment as an unrecognized reservoir for community-associated methicillin resistant *Staphylococcus aureus* USA300: a case-control study. PLoS One **6:**e22407. doi:10.1371/journal.pone.0022407.
29. **Gray RR, Tatem AJ, Johnson JA, Alekseyenko AV, Pybus OG, Suchard MA, Salemi M.** 2011. Testing spatiotemporal hypothesis of bacterial evolution using methicillin-resistant *Staphylococcus aureus* ST239 genome-wide data within a bayesian framework. Mol. Biol. Evol. **28:**1593–1603.
30. **McAdam PR, Templeton KE, Edwards GF, Holden MT, Feil EJ, Aanensen DM, Bargawi HJ, Spratt BG, Bentley SD, Parkhill J, Enright MC, Holmes A, Girvan EK, Godfrey PA, Feldgarden M, Kearns AM, Rambaut A, Robinson DA, Fitzgerald JR.** 2012. Molecular tracing of the emergence, adaptation, and transmission of hospital-associated methicillin-resistant *Staphylococcus aureus*. Proc. Natl. Acad. Sci. U. S. A. **109:**9107–9112.
31. **El Baze P, Milano G, Verrando P, Renée N, Ortonne JP.** 1983. Polyamine levels in normal human skin. A comparative study of pure epidermis, pure dermis, and suction blister fluid. Arch. Dermatol. Res. **275:**218–221.
32. **Lauderdale KJ, Boles BR, Cheung AL, Horswill AR.** 2009. Interconnections between sigma B, *agr*, and proteolytic activity in *Staphylococcus aureus* biofilm maturation. Infect. Immun. **77:**1623–1635.
33. **Boles BR, Horswill AR.** 2008. Agr-mediated dispersal of *Staphylococcus aureus* biofilms. PLoS Pathog. **4:**e1000052. doi:10.1371/journal.ppat.1000052.
34. **Periasamy S, Joo HS, Duong AC, Bach TH, Tan VY, Chatterjee SS, Cheung GY, Otto M.** 2012. How *Staphylococcus aureus* biofilms develop their characteristic structure. Proc. Natl. Acad. Sci. U. S. A. **109:**1281–1286.
35. **Vuong C, Saenz HL, Götz F, Otto M.** 2000. Impact of the agr quorum-sensing system on adherence to polystyrene in *Staphylococcus aureus*. J. Infect. Dis. **182:**1688–1693.
36. **Yarwood JM, Bartels DJ, Volper EM, Greenberg EP.** 2004. Quorum sensing in *Staphylococcus aureus* biofilms. J. Bacteriol. **186:**1838–1850.
37. **O'Neill E, Pozzi C, Houston P, Humphreys H, Robinson DA, Loughman A, Foster TJ, O'Gara JP.** 2008. A novel *Staphylococcus aureus* biofilm phenotype mediated by the fibronectin-binding proteins, FnBPA and FnBPB. J. Bacteriol. **190:**3835–3850.
38. **Rice KC, Mann EE, Endres JL, Weiss EC, Cassat JE, Smeltzer MS, Bayles KW.** 2007. The cidA murein hydrolase regulator contributes to DNA release and biofilm development in *Staphylococcus aureus*. Proc. Natl. Acad. Sci. U. S. A. **104:**8113–8118.
39. **Cramton SE, Gerke C, Schnell NF, Nichols WW, Götz F.** 1999. The intercellular adhesion (*ica*) locus is present in *Staphylococcus aureus* and is required for biofilm formation. Infect. Immun. **67:**5427–5433.
40. **Houston P, Rowe SE, Pozzi C, Waters EM, O'Gara JP.** 2011. Essential role for the major autolysin in the fibronectin-binding protein-mediated *Staphylococcus aureus* biofilm phenotype. Infect. Immun. **79:**1153–1165.
41. **McDevitt D, Nanavaty T, House-Pompeo K, Bell E, Turner N, McIntire L, Foster T, Höök M.** 1997. Characterization of the interaction between the *Staphylococcus aureus* clumping factor (ClfA) and fibrinogen. Eur. J. Biochem. **247:**416–424.
42. **Wann ER, Gurusiddappa S, Hook M.** 2000. The fibronectin-binding MSCRAMM FnbpA of *Staphylococcus aureus* is a bifunctional protein that also binds to fibrinogen. J. Biol. Chem. **275:**13863–13871.
43. **Signäs C, Raucci G, Jönsson K, Lindgren PE, Anantharamaiah GM, Höök M, Lindberg M.** 1989. Nucleotide sequence of the gene for a fibronectin-binding protein from *Staphylococcus aureus*: use of this peptide sequence in the synthesis of biologically active peptides. Proc. Natl. Acad. Sci. U. S. A. **86:**699–703.
44. **Bernier SP, Létoffé S, Delepierre M, Ghigo JM.** 2011. Biogenic ammonia modifies antibiotic resistance at a distance in physically separated bacteria. Mol. Microbiol. **81:**705–716.
45. **Menzies BE, Kenoyer A.** 2005. *Staphylococcus aureus* infection of epidermal keratinocytes promotes expression of innate antimicrobial peptides. Infect. Immun. **73:**5241–5244.
46. **Midorikawa K, Ouhara K, Komatsuzawa H, Kawai T, Yamada S, Fujiwara T, Yamazaki K, Sayama K, Taubman MA, Kurihara H, Hashimoto K, Sugai M.** 2003. *Staphylococcus aureus* susceptibility to innate antimicrobial peptides, beta-defensins and CAP18, expressed by human keratinocytes. Infect. Immun. **71:**3730–3739.
47. **Kisich KO, Howell MD, Boguniewicz M, Heizer HR, Watson NU, Leung DY.** 2007. The constitutive capacity of human keratinocytes to kill *Staphylococcus aureus* is dependent on beta-defensin 3. J. Invest. Dermatol. **127:**2368–2380.
48. **Yu H, Wier L, Elixhauser A.** 2011. Hospital stays for children, 2009, HCUP statistical brief 118. Agency for Healthcare Research and Quality, Rockville, MD. http://www.hcup-us.ahrq.gov/reports/statbriefs/sb118.pdf.
49. **Vlassova N, Han A, Zenilman JM, James G, Lazarus GS.** 2011. New horizons for cutaneous microbiology: the role of biofilms in dermatological disease. Br. J. Dermatol. **165:**751–759.
50. **Kolodkin-Gal I, Cao S, Chai L, Böttcher T, Kolter R, Clardy J, Losick R.**

Downloaded from https://journals.asm.org/journal/mbio on 25 August 2022 by 138.5.97.228.

2012. A self-produced trigger for biofilm disassembly that targets exopolysaccharide. Cell **149:**684–692.
51. **Clark RA.** 1990. Fibronectin matrix deposition and fibronectin receptor expression in healing and normal skin. J. Invest. Dermatol. **94:**128S–134S.
52. **Drew AF, Liu H, Davidson JM, Daugherty CC, Degen JL.** 2001. Wound-healing defects in mice lacking fibrinogen. Blood **97:**3691–3698.
53. **Schwarz-Linek U, Höök M, Potts JR.** 2004. The molecular basis of fibronectin-mediated bacterial adherence to host cells. Mol. Microbiol. **52:**631–641.
54. **Li M, Diep BA, Villaruz AE, Braughton KR, Jiang X, DeLeo FR, Chambers HF, Lu Y, Otto M.** 2009. Evolution of virulence in epidemic community-associated methicillin-resistant *Staphylococcus aureus*. Proc. Natl. Acad. Sci. U. S. A. **106:**5883–5888.
55. **Montgomery CP, Boyle-Vavra S, Daum RS.** 2010. Importance of the global regulators Agr and SaeRS in the pathogenesis of CA-MRSA USA300 infection. PLOS ONE **5:**e15177. doi:10.1371/journal.pone.0015177.
56. **Edgar RC.** 2004. MUSCLE: multiple sequence alignment with high accuracy and high throughput. Nucleic Acids Res. **32:**1792–1797.
57. **Tamura K, Peterson D, Peterson N, Stecher G, Nei M, Kumar S.** 2011. MEGA5: molecular evolutionary genetics analysis using maximum likelihood, evolutionary distance, and maximum parsimony methods. Mol. Biol. Evol. **28:**2731–2739.
58. **Ronquist F, Huelsenbeck JP.** 2003. MrBayes 3: bayesian phylogenetic inference under mixed models. Bioinformatics **19:**1572–1574.
59. **Stamatakis A.** 2006. RAxML-VI-HPC: maximum likelihood-based phylogenetic analyses with thousands of taxa and mixed models. Bioinformatics **22:**2688–2690.
60. **Drummond AJ, Suchard MA, Xie D, Rambaut A.** 2012. Bayesian phylogenetics with BEAUti and the BEAST 1.7. Mol. Biol. Evol. **29:**-1969–1973.
61. **Drummond AJ, Ho SY, Phillips MJ, Rambaut A.** 2006. Relaxed phylogenetics and dating with confidence. PLoS Biol. **4:**e88. doi:10.1371/journal.pbio.0040088.
62. **Geoghegan JA, Monk IR, O'Gara JP, Foster TJ.** 2013. Subdomains N2N3 of fibronectin binding protein A mediate *Staphylococcus aureus* biofilm formation and adherence to fibrinogen using distinct mechanisms. J. Bacteriol. **195:**2675–2683.
63. **Kulkarni R, Antala S, Wang A, Amaral FE, Rampersaud R, Larussa SJ, Planet PJ, Ratner AJ.** 2012. Cigarette smoke increases *Staphylococcus aureus* biofilm formation via oxidative stress. Infect. Immun. **80:**3804–3811.

Downloaded from https://journals.asm.org/journal/mbio on 25 August 2022 by 138.5.97.228.